# Advanced Operational Modal Analysis Methods for Linear Time Periodic System Identification

**Mathew S. Allen,**
*Department of Engineering Physics*
*University of Wisconsin*
*Madison, WI 53706*
msallen@engr.wisc.edu

**Shashank Chauhan**
*Brüel & Kjær*
*Sound & Vibration Measurement A/S*
*Skodsborgvej 307*
*DK-2850 Nærum, Denmark*
schauhan@bksv.com

*&*

**Morten Hartvig Hansen**
*Wind Energy Department*
*Risø National Laboratory*
*P.O. Box 49, DK-4000 Roskilde*
*Denmark*

## ABSTRACT

Often structural dynamic systems cannot be modeled with constant stiffness, mass and damping. For example, wind turbines, helicopters, turbomachinery, and a variety of nonlinear structures linearized about a periodic limit cycle all may contain time-periodic terms in their equations of motion even if the equations are still linear. Linear time periodic systems such as these may exhibit parametric resonance, where the damping in the system is negative at certain rotational frequencies, leading to catastrophic failure. The authors previously presented an extension of operational modal analysis to linear time periodic systems. The previous work introduced a new type of spectrum, dubbed the harmonic autospectrum, discussed how to interpret the spectra, and showed how the simple peak picking method could be used to extract an estimate for the linear time-periodic model of a system from measurements. This paper builds on that work, revealing how more advanced operational modal analysis methods can be extended to linear time-periodic systems. Curve fitting approaches for both the harmonic autospectra and the positive harmonic spectra are applied to simulated measurements from two time-periodic systems, and the OMA based Enhanced Mode Indicator Function (EMIF) method is used to extract the modal parameters from the enhanced positive power spectrum. These extensions are found to provide more accurate estimates of the damping of the modes of the time-periodic systems, and to provide good estimates of the mode shapes of the systems so long as the measurements stand out clearly above the noise. Application of the complex mode indicator function an the EMIF algorithm makes it possible to separate the forward and backward whirling modes of a wind turbine, which is difficult since each of these modes is manifest at several harmonics due to the anisotropy in the tower supporting the turbine.

## 1. INTRODUCTION

Many important structural systems require time-varying terms in their equations of motion. For example, the stiffness matrix of a two-bladed wind turbine [1] or any wind turbine with non-identical blades [2] depends on the angle of the rotor, and if the rotor speed is constant the equations of motion become linear time periodic (LTP). Linear time periodic equations of motion are commonly used to model other kinds of rotating machinery [3], for studying the stability of various classes of nonlinear systems linearized about a periodic limit cycle , and they have also been used to accelerate laser Doppler vibrometry measurements using the Continuous Scan (CSLDV) approach [4].

In a prior work, the authors presented a operational modal analysis (OMA) methodology for linear time periodic systems and validated it using simulated measurements from a Mathieu oscillator and a rotating wind turbine [5, 6]. Measurements from the latter were simulated using HAWC2 [7], a high fidelity simulation code that includes the random loading that the wind applies to the rotating turbine. The LTP-OMA methodology was subsequently applied to continuous scan laser vibrometry measurements from a few different structures [8], revealing that the methodology is capable of extracting detailed mode shapes from real experimental measurements.

The authors' original work [5, 6] presented the LTP-OMA methodology and focused on interpreting spectral measurements from the time-periodic systems. The simple peak-picking method was used to extract time-periodic models of the systems from the autospectrum of the output. Several more advanced techniques exist for interrogating and curve fitting operational modal analysis measurements from linear time invariant systems. This work shows how some of those methods can be applied to measurements from linear time periodic systems. Methods for curve fitting the spectra to a modal model, both the full harmonic power spectra as well as the positive harmonic spectra, and the two methods are compared. The OMA based Enhanced Mode Indicator Function (EMIF) method [9], an extension to the complex mode indicator function (CMIF) is also applied to the measurements and its performance is evaluated.

The following section reviews the LTP-OMA identification methodology and shows how the advanced OMA methods can be adapted to measurements from the time periodic system. In Section 3 the methods are applied to simulated measurements from two linear time periodic systems, a Mathieu oscillator and a 5MW wind turbine in operation. Section 4 presents the conclusions.

## 2. THEORY

The state space equations of motion of a linear time-periodic (LTP) system can be written as follows,

$$\begin{aligned} \dot{x} &= A(t)x + B(t)u \\ y &= C(t)x + D(t)u \end{aligned} \tag{1}$$

where $A(t+T_A) = A(t)$ and the other matrices are periodic as well with the same period. The fundamental frequency of the time-periodic system is denoted $\omega_A = 2\pi/T_A$. The state transition matrix (STM) [10] gives the free response of such a system at time $t$ via the relationship,

$$x(t) = \Phi(t, t_0)x(t_0)\,. \tag{2}$$

One can also write the forced response of the system in terms of the STM as follows.

$$y(t) = C(t)\Phi(t, t_0)x(t_0) + \int_{t_0}^{t} C(t)\Phi(t, \tau)B(\tau)u(\tau)d\tau \tag{3}$$

In the absence of degenerate roots, the state transition matrix of an LTP system can be represented as a modal sum [11, 12],

$$\Phi(t,t_0) = \sum_{r=1}^{N} \psi_r(t) L_r(t_0)^T e^{\lambda_r (t-t_0)} \tag{4}$$

where $\lambda_r$ is the $r$th Floquet exponent of the state transition matrix, $\psi_r$ is the $r$th time-periodic mode vector of the STM and $L_r$ is the $r$th column of $\Psi(t) = \begin{bmatrix} \psi_1(t) & \psi_2(t) & \cdots \end{bmatrix}^{-T}$. The Floquet exponents of an LTP system are analogous to the eigenvalues of a Linear Time Invariant (LTI) system, which can be written in terms of the damping ratio $\zeta_r$ and natural frequency $\omega_r$ as $\lambda_r = -\zeta_r \omega_r + \mathrm{i}\omega_r \sqrt{1-\zeta_r^{\,2}}$ for an underdamped mode.

In a prior work [5, 6], the authors used this equation to derive an expression for the output auto spectrum of a linear time periodic system in terms of the modal parameters of the state transition matrix. In order to achieve this, first an exponentially modulated version of the output signal is developed as follows,

$$\mathbf{Y}(\omega) = \begin{bmatrix} \cdots & y_{-1}(\omega)^{\mathrm{T}} & y_0(\omega)^{\mathrm{T}} & y_1(\omega)^{\mathrm{T}} & \cdots \end{bmatrix}^{\mathrm{T}} \tag{5}$$

where

$$y_n(\omega) = \int_{-\infty}^{\infty} y(t) e^{(-\mathrm{i}\omega - \mathrm{i}n\omega_A)t} dt \tag{6}$$

is simply the Fourier transform of $y(t)$, shifted in frequency by $n\omega_A$ where $n$ is an integer. Then, the harmonic autospectrum $S_{yy}(\omega) = \mathrm{E}\left(\mathbf{Y}(\omega)\mathbf{Y}(\omega)^H\right)$ is given by the following equation when $D(t) = 0$.

$$\left[S_{yy}(\omega)\right] = \sum_{r=1}^{N} \sum_{l=-\infty}^{\infty} \sum_{s=1}^{N} \sum_{k=-\infty}^{\infty} \frac{\bar{\mathbf{C}}_{r,l} \mathbf{W}(\omega)_{r,s,l,k} \bar{\mathbf{C}}_{s,k}^{\;H}}{\left[\mathrm{i}\omega - (\lambda_r - \mathrm{i}l\omega_A)\right]\left[\mathrm{i}\omega - (\lambda_s - \mathrm{i}k\omega_A)\right]^H} \tag{7}$$

The matrix $\mathbf{W}(\omega)$ is a function of the input spectrum and is assumed to be reasonably flat. The dominant terms in the summation above are those for which $\mathrm{i}\omega - (\lambda_r - \mathrm{i}l\omega_A)$ and $\mathrm{i}\omega - (\lambda_s - \mathrm{i}k\omega_A)$ are both minimum at the same frequency. If the sidebands for mode $r$ do not overlap with those for mode $s$, then the largest terms occur when $r$=$s$ and $l$=$k$ and the expression becomes the following.

$$\left[S_{yy}(\omega)\right] \approx \sum_{r=1}^{N} \sum_{l=-\infty}^{\infty} \frac{\bar{\mathbf{C}}_{r,l} \mathbf{W}(\omega)_{r,l} \bar{\mathbf{C}}_{r,l}^{\;H}}{\left[\mathrm{i}\omega - (\lambda_r - \mathrm{i}l\omega_A)\right]\left[\mathrm{i}\omega - (\lambda_r - \mathrm{i}l\omega_A)\right]^H} \tag{8}$$

This is a summation of terms with $\left(\mathrm{i}\omega - \lambda\right)\left(\mathrm{i}\omega - \lambda\right)^H$ in the denominator, or squared modal contributions, so the harmonic autospectrum has the same mathematical form as the output autospectrum of a multi-output linear time invariant system. However, there are a few important differences. First, the expression contains a summation over both the modes, whose eigenvalues are $\lambda_r$, and also a summation over the harmonics of $\omega_A$ using the integer index $l$. As a result, the autospectrum of the LTP system will have peaks near each natural frequency, $\omega_r$, and also at the frequencies $\omega_r \pm l\omega_A$ for any integer $l$. Second, the mode vectors $\bar{\mathbf{C}}_{r,l}$ are actually the Fourier coefficients of the time-varying mode shapes of the LTP system as discussed in [5, 6]. These vectors could have infinite dimension, but in practice some finite number of terms $N_p$ is

sufficient to accurately describe the mode shape. Hence, if the system as $N_o$ outputs, then the vectors $\bar{\mathbf{C}}_{r,l}$ have length $N_o \times N_p$, where $N_p$ is the number of modulations used to form $\mathbf{Y}(\omega)$ in eq. (5). Many different vectors $\bar{\mathbf{C}}_{r,l}$ can be identified, but each contains the same Fourier coefficients of the observed mode vectors shifted by $l$. Specifically, if the time varying mode shape at the output is

$$C(t)\psi_r(t) = \sum_{n=-\infty}^{\infty} \bar{C}_{r,n} e^{jn\omega_A t} \tag{9}$$

then $\bar{\mathbf{C}}_{r,l}$ is given by.

$$\bar{\mathbf{C}}_{r,l} = \begin{bmatrix} \cdots & \bar{C}_{r,-1-l}{}^T & \bar{C}_{r,-l}{}^T & \bar{C}_{r,1-l}{}^T & \cdots \end{bmatrix}^T \tag{10}$$

Additional details of this theory can be found in [5, 6].

In a previous work [5], the authors used the peak picking method together with the expressions developed above to estimate the natural frequencies and the mode vectors $\bar{\mathbf{C}}_{r,l}$ of the LTP system. This work explores other more advanced methods, including curve fitting and advance spatial domain tools, such as CMIF, based methods for the purpose of modal parameter estimation of LTP systems.

### 2.1. Curve fitting autospectra

Since the harmonic autospectrum, (or equivalently harmonic power spectral density, here denoted HPSD) of an LTP system was shown in eq. (8) to have same mathematical form as an LTI system (i.e. it is a summation of modal contributions squared), it can be put into a convenient form for curve fitting. Assuming underdamped modes $\lambda_{r+(N/2)} = \lambda_r^*$, where ()* denotes complex conjugate, and contribution due to each underdamped mode can be collected and written as follows after a partial fraction expansion.

$$\left[S_{yy}(\omega)\right] \approx \sum_{r=1}^{N/2} \sum_{l=-\infty}^{\infty} \frac{\mathbf{A}_{r,l}}{\left[\mathrm{i}\omega - (\lambda_r - \mathrm{i}l\omega_A)\right]} + \frac{\mathbf{A}^*_{r,l}}{\left[\mathrm{i}\omega - (\lambda_r - \mathrm{i}l\omega_A)^*\right]} + \frac{\mathbf{B}_{r,l}}{\left[-\mathrm{i}\omega - (\lambda_r - \mathrm{i}l\omega_A)\right]} + \frac{\mathbf{B}^*_{r,l}}{\left[-\mathrm{i}\omega - (\lambda_r - \mathrm{i}l\omega_A)^*\right]} \tag{11}$$

Alternatively, this could be written as a matrix polynomial model with complex coefficients in even powers of (iω). Various algorithms can fit a model of this form to a set of measurements. For this work the Algorithm of Mode Isolation (AMI) [13] was modified to fit a model of the form described above and used to extract modes from the harmonic autospectrum.

### 2.2. Positive Power Spectra

The power spectrum of a signal possesses four quadrant symmetry, and hence it includes information of system poles twice. This can also be seen in eq. (11), which contains each of the poles, once having positive damping and other having negative damping (note that same is true for the complex conjugate pole as well). These extra negatively damped poles can lead to difficulty when estimating the modal parameters of the system.

This problem can be dealt with by considering positive power spectra instead of power spectra. The inverse FFT of the power spectrum is found, and then a rectangular window is used in the time domain to eliminate the negatively damped modes by retaining only the decaying part of the impulse response function. Thus PPS functions have the same form as a typical frequency response function (FRF) has, making them more suitable for modal parameter estimation. The process of estimating PPS functions from power spectra is described in detail in [9].

In this work, the same approach is used to convert a set of harmonic power spectra into positive harmonic power spectra. Once this has been done, the negatively damped poles are no

longer present and the positive harmonic power spectrum (pHPSD or $S^{+}{}_{yy}(\omega)$) can be written in the following mathematical form.

$$\left[S^{+}{}_{yy}(\omega)\right] \approx \sum_{r=1}^{N/2} \sum_{l=-\infty}^{\infty} \frac{\mathbf{A}_{r,l}}{\left[\mathrm{i}\omega - (\lambda_r - \mathrm{i}l\omega_A)\right]} + \frac{\mathbf{A}^{*}{}_{r,l}}{\left[\mathrm{i}\omega - (\lambda_r - \mathrm{i}l\omega_A)^{*}\right]} \tag{12}$$

The pHSPD has the usual magnitude and phase relationship as a frequency response function, so it can often be more accurately curve fit. In the following the AMI algorithm in [13, 14] was used to fit a model of the form above to the power spectra in order to construct the time periodic modes of the system. Since the pHSPD has the same mathematical form as a frequency response function, no modification to the AMI algorithm was necessary when doing this.

### 2.3. EMIF based Method

The enhanced mode indicator function (EMIF) method was proposed for operational modal analysis in [9]. Here that approach is adapted to parameter estimation on harmonic power spectral measurements (HPSD). OMA-EMIF method works on positive power spectra, which are defined in section 2.2. One begins by choosing a frequency range of interest and also the number of modes to be identified in the chosen frequency range. The number of modes to be identified is typically equal to the number of dominant peaks in the CMIF plot over the chosen frequency range. The positive power spectra in the chosen frequency range are then assembled in an augmented matrix form as shown below, where $N_{tot}$ is the number of responses and $N_f$ is number of frequency lines in chosen frequency range. For an LTP system there are $N_p$ responses for each measurement point, so $N_{tot}=N_oN_p$.

$$\left[A_0\right]_{N_{tot} \times (N_{tot}N_f)} = \begin{bmatrix} S^{+}_{11}(\omega_i) & \cdots & S^{+}_{11}(\omega_{i+N_f}) & \cdots & S^{+}_{21}(\omega_i) & \cdots & S^{+}_{21}(\omega_{i+N_f}) & \cdots & S^{+}_{p1}(\omega_i) & \cdots & S^{+}_{p1}(\omega_{i+N_f}) \\ \vdots & \vdots & \vdots & \vdots & \vdots & \vdots & \vdots & \vdots & \vdots & \vdots & \vdots \\ S^{+}_{pq}(\omega_i) & \cdots & S^{+}_{pq}(\omega_{i+N_f}) & \cdots & \cdots & \cdots & \cdots & \cdots & \cdots & \cdots & S^{+}_{pq}(\omega_{i+N_f}) \end{bmatrix} \tag{13}$$

This matrix now has all of the spatial information contained in the autospectrum, over all of the frequency lines that have been included in $[A_0]$. A singular value decomposition of this augmented matrix yields left and right singular vectors along with the singular values. Supposing that $N_b$ modes are to be indentified from the measurements, the first $N_b$ dominant left singular vectors are chosen to create an enhanced positive power spectra in the chosen frequency range of interest. This is shown in below, where $[U]$ is a matrix of left singular vectors of the augmented matrix.

$$ePPS(\omega) = \left[\overline{S}(\omega)\right]_{N_b \times N_{tot}} = [U]^{T}_{N_b \times N_{tot}} \left[S^{+}(\omega)\right]_{N_{tot} \times N_{tot}} \tag{14}$$

The ePPS functions can now be used to identify the $N_b$ modes by applying a single degree-of-freedom unified matrix polynomial [15] algorithm to each of the peaks in the ePPS. The modal vectors obtained from ePPS functions are in a condensed set of coordinates and can be converted back into physical domain by pre-multiplying the obtained modal vectors with $\left[U\right]_{N_b \times N_{tot}}$.

## 3. Simulated Application Examples

### 3.1. Mathieu Oscillator

This section applies the proposed methodologies to two different systems. The first is the simple Mathieu oscillator, a spring mass-damper system with time-periodic spring stiffness. The equation of motion for the oscillator is

$$\ddot{y} + 2\zeta\omega_0\dot{y} + \left(\omega_0^2 + \omega_1^2\cos(\omega_A t)\right)y = \frac{u(t)}{m} \tag{15}$$

with $2\zeta\omega_0 = c/m$, $\omega_0^2 = k_0/m$, $\omega_1^2 = k_1/m$, and input *u(t)*. The parameters used in this work are the following, $m$=1, $k_0$=1, $k_1$=0.4, and $\omega_A$=0.8 rad/s, which are the same as those used in [5, 6].

### *3.1.1. Curve Fitting HPSD*

The response of the Mathieu oscillator to a broadband random input was simulated using time integration, and the harmonic autospectrum (HPSD) was then computed with $p$=2, so $n$ = -2…2 in eq. (6) so $N_p$=5 and a 5x5 HPSD matrix was produced. The primary column of this matrix (i.e. the $(p+1)^{th}$ or 3rd column in this case) contains all of the information needed to identify the parameters of the system, so only it will be considered in the curve fit. The composite [13], or average, of this 5x1 matrix is shown in Figure 1 with a black line. The composite of a curve fit is also shown as well as the difference between the two. The curve fit can be seen to follow the measurements closely near each of the peaks in the spectrum, but the baseline level of the curve fit is too high so the highest frequency peak is almost obscured by the tails of the dominant modes.

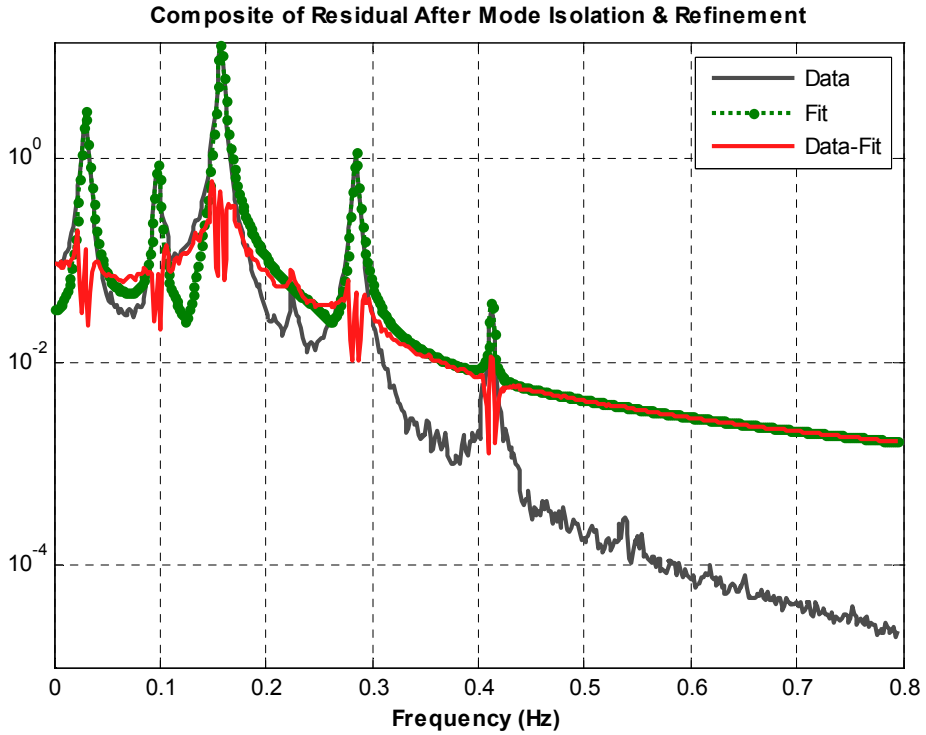


*Figure 1: Harmonic Autospectrum of Mathieu Oscillator response with: (black line) composite of actual autospectrum, (green dotted) curve fit to the HPSD and (red) composite of the difference between the curve fit and the measurements.*

The authors have seen this same phenomena occur when fitting conventional autospectra of structural systems. For those systems the curve fitting routine seems to ascribe more complexity to the modes than is warranted. Better results can sometimes be obtained if the curve fitting routine is forced to fit a real mode model to the measurements, but that is not possible for measurements from an LTP system since the HPSD must be fit to a complex mode model. The

authors also noted that the damping obtained for each of the modes seemed to be somewhat sensitive to the number of points around each peak that was used in the curve fit.

### *3.1.2. Curve Fit to Positive HPSD ($S_{yy}^{+}$)*

The positive power spectra of the measurements were formed as discussed in Section 2.2. Figure 2 shows a composite of the 5x1 positive power spectrum in the same format used in the previous figure, as well as a curve fit. The positive power spectrum seems to be smoother than the full HSPD, and the fit agrees very well with the measurements. The residual (red line) is small and seems to contain only noise, suggesting that the curve fit has extracted all of the meaningful information from the measurement. The results of the curve fits shown in Figures 1 and 2 are summarized in Table 1, which will be discussed later.

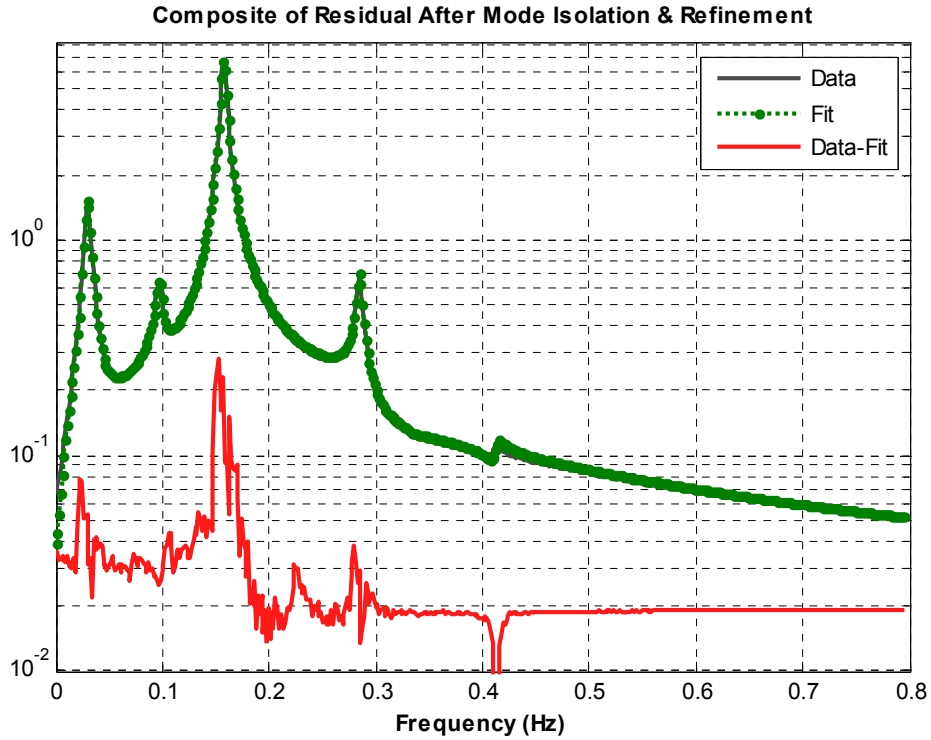


*Figure 2: Positive Harmonic Autospectrum ($S_{yy}^{+}$) of Mathieu Oscillator response with: (black line) composite of actual autospectrum, (green dotted) curve fit to the HPSD and (red) composite of the difference between the curve fit and the measurements.*

### *3.1.3. Application of OMA-EMIF Method to HPSD*

The OMA-EMIF method was also applied to the simulated measurements from the Mathieu oscillator. In doing so, the full power spectrum matrix for $p$=2 was used (rather than the column used in the previous two subsections). A CMIF plot was first created from the HPSD matrix, which is shown in Figure 3. The CMIF plot is far more convenient to view than the individual elements of the harmonic power spectrum matrix, which were shown in [5, 6], yet it retains information regarding the mode shapes of the system that can be used to detect modes with close natural frequencies. In this plot, the peak at 0.982 Hz is the Floquet exponent of the system and other peaks of the same amplitude that appear in the plot are modulations of the Floquet exponent, $\lambda+in\omega_A$, for $n$ = -2,…2, where $\omega_A$=0.8 rad/s. Other weaker peaks are also visible in the CMIF for other values of $n$.

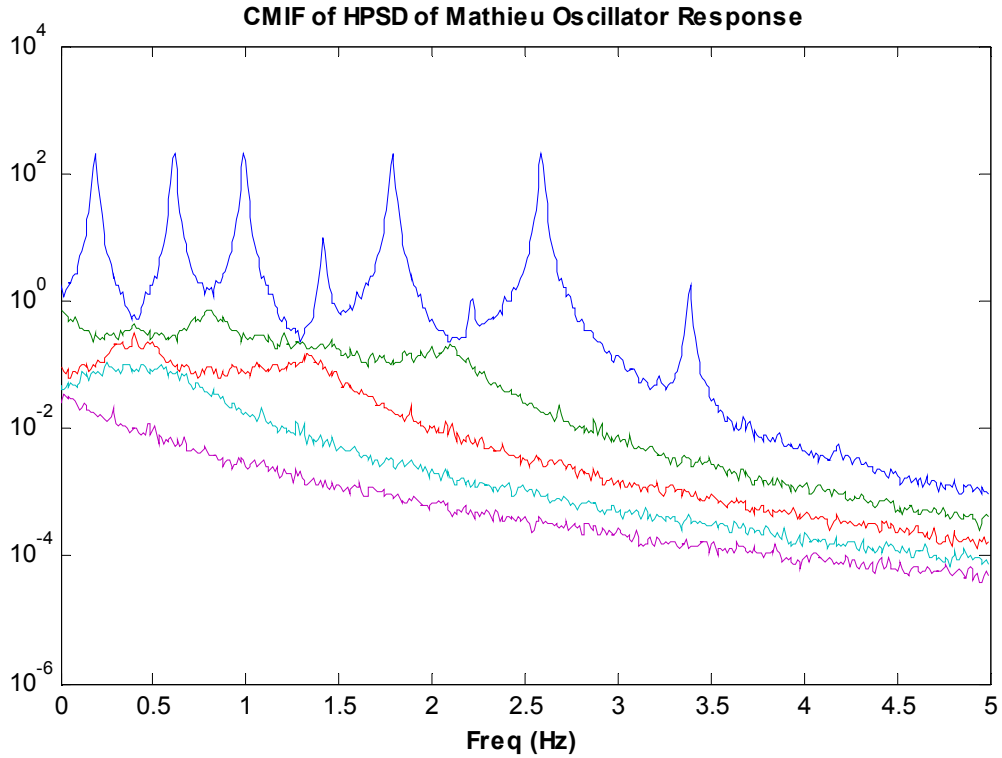


*Figure 3: CMIF of the HPSD of the Mathieu oscillator response. The individual curves correspond to different singular values of the HPSD matrix at each frequency.*

The EMIF methodology was then applied to the measurements, by creating the enhanced positive power spectrum and then fitting low-order modal models to them. The modal paramters of each of the peaks were identified, but for brevity only the mode identified at the 0.982 Hz peak will be considered.

### *3.1.4 Comparison of Numerical Results*

Table 1 shows the result of parameter estimation using various methods. The column labeled "Peak Picking" shows the result obtained by peak picking, which was previously published in [6]. Each of the peaks in the HPSD, pHPSD and CMIF were fit by each method, and they all may contain useful information regarding the mode shapes and eigenvalues of the LTP system. However, for brevity only the result obtained from the primary peak near 0.98 rad/s is compared.

| $n$ | *Fourier Coefficients of the Mathieu Oscillator Mode Shape* $\overline{C}_{1,n}$ | | | | |
|---|---|---|---|---|---|
| | **Analytical** | **Peak Picking** | **Fit to Harmonic PSD** | **Fit to Positive HPSD** | **OMA-EMIF** |
| **-2** | 0.067 | 0.0650 - 0.0090i | 0.0667 + 0.00233i | 0.0652 + 0.00095i | 0.063 – 0.014i |
| **-1** | -0.220 | -0.220 + 0.0061i | -0.217 - 0.00151i | -0.219 - 0.00113i | -0.219+0.009i |
| **0** | 1 | 1 | 1 | 1 | 1 |
| **1** | 0.092 | 0.0906 + 0.0011i | 0.0910 - 0.00126i | 0.0902 - 0.00212i | 0.094 + 0.001i |
| **2** | 0.00320 | 0.0028 - 0.0001i | 0.00340 +0.00050i | 0.00308 +0.00029i | 0.003 + 0.0004i |
| **$\lambda$** | -0.0200 + 0.987i | -0.0270 +0.986i | -0.0169 +0.987i | -0.0172 + 0.988i | -0.0124 + 0.988i |
| **$\omega_n$** | 0.987 | 0.986 | 0.987 | 0.988 | 0.988 |
| **$\zeta$** | 0.0203 | 0.0274 | 0.0171 | 0.0174 | 0.0123 |

*Table 1: Mode shape coefficients identified at the fundamental peak using various methods. The analytical vector* $\overline{\mathbf{C}}_{1,0}$ *is shown in the first column.*

The results obtained by each of these methods are quite similar. The only large discrepancy between the methods occurs for the damping ratio, which is poorly estimated using the peak picking method as expected. The results obtained using the HPSD and the positive HPSD seem to have similar quality, even though the curve fit on the positive power spectrum seemed to be far more satisfying. The OMA-EMIF agrees well with the other two curve-fitting methods.

The result is somewhat surprising if the fit to one of the weak peaks is compared. Table 2 compares the Fourier coefficients obtained at the 2.6 rad/s peak in Figures 1 and 2. This peak was very weakly represented in the measurements, and was seen to be almost buried in the residual in the HPSD curve fit in Figure 1. The estimates of the Fourier coefficients produced by the peak picking method are up to four times larger than the true coefficients, but the curve fitting methods give results with even greater errors. This anomaly is readily explained. The measurements from which the coefficients 2, 3 and 4 were obtained were plotted (not shown here) and it was observed that none of those measurements showed any visual evidence of a mode near 2.6 rad/s. The spurious values seen in the table seem to arise as the least squares procedure attempts to fit a mode to the shoulder of one of the more prominent peaks. On the other hand, a weak peak was visible in the measurement from which the $n$=1 coefficient was estimated, but even there the peak picking method seems to have achieved a better estimate of the Fourier coefficient.

| $n$ | *Fourier Coefficients of the Mathieu Oscillator Mode Shape* $\overline{C}_{1,n}$ | | | |
|---|---|---|---|---|
| | **Analytical** | **Peak Picking** | **Fit Harmonic PSD** | **Fit Positive HPSD** |
| **0** | 1 | 1 | 1 | 1 |
| **1** | 0.092 | 0.0918 + 0.00090i | 0.0626 + 0.0246i | -0.0701 + 0.00662i |
| **2** | 0.003197 | 0.0136 - 0.00054i | -0.32764 + 0.055243i | 0.940 + 0.184i |
| **3** | 0.000039 | 0.000824 - 0.000289i | -0.0137 - 0.0133i | -0.112 - 0.0409i |
| **4** | -0.000015 | 0.000053 - 0.00021i | -0.000688 + 0.00072i | -0.0152 - 0.00348i |
| **$\lambda$** | -0.0200 + 2.587i | - | -0.0185 + 2.592i | -0.0223 + 2.593i |
| **$\omega_n$** | 2.587 | 2.588 | 2.592 | 2.593 |

*Table 2: Mode shape coefficients identified at the 2.6 rad/s peak in the HPSD and pHPSD using various methods.*

### 3.2. Simulated Measurements from a Wind Turbine

This section applies the proposed LTP system identification methods to a much more challenging problem, a 5MW wind turbine rotating at constant speed due to aerodynamic forcing. Turbulence in the incoming wind provides a source of broadband random excitation. The system and conditions studied here are identical to those reported in the authors' prior work [5, 6], where peak picking was used to identify the edgewise modes of the turbine. In that work, some difficulty was reported in distinguishing the forward and backward whirling modes of the turbine since many of their harmonics overlap. Here the advanced LTP system identification algorithms will be applied to that system in an effort to enhance the results. The wind turbine is rotating at a constant rate of 0.201 Hz in these measurements, driven by a wind with logarithmic shear with 18 m/s velocity at hub height.

Measurement of the edgewise motion of each of the three blades was simulated, as well as lateral and fore-aft motion of the tip of the tower. The harmonic autospectrum matrix was computed for these five measurements with $n$=-2…2. The total measurement set is quite difficult to visualize, so two separate CMIFs were created, shown in Figures 4 and 5. Figure 4 shows a CMIF including the two measurement points on the tower and all of their harmonics. As with the results in the previous section, only the primary column of the HPSD matrix was used, so the CMIF is based on a 10x2 matrix. The CMIF clearly shows the presence of the first two modes of the tower, both near 0.27 Hz. The forward whirling mode of the rotor is also visible at 1.16 Hz, and there is a very small peak near 0.76 Hz, where the corresponding backward whirling mode should be. A harmonic of the forward mode also seems to be visible near 1.36 Hz. Finally, there is a large triangular shaped peak in the spectrum near the blade-pass frequency of 0.6 Hz. This is due to the aerodynamic forcing function of the system and is not a mode of the structure, as discussed in [6, 16].

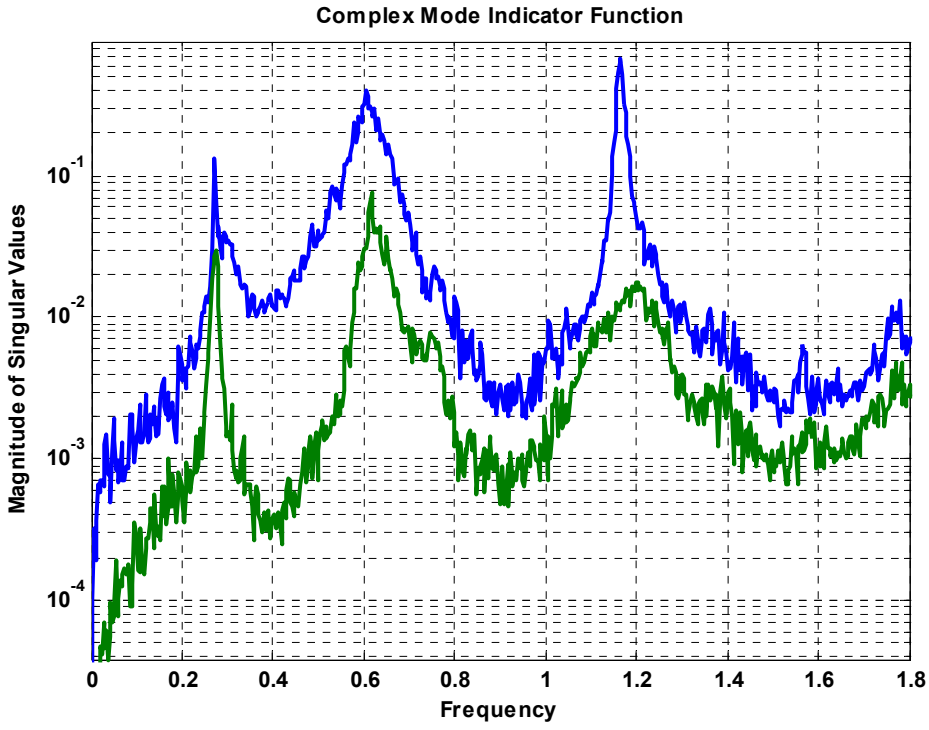


*Figure 4: CMIF of the HPSD for tower motion of wind turbine.*

Figure 5 shows the CMIF using the three edgewise blade measurements as references. In this spectrum, contamination is clearly visible at the rotor speed and its harmonics: 0.2 Hz, 0.4

Hz, 0.6 Hz and (diminished) at 0.8 Hz. The dominant peaks in the spectrum are the edgewise modes of the turbine near 0.96 Hz. These are the same forward and backward whirling modes that were seen in Figure 4, but the blade measurements were taken in the rotating reference frame so those two modes appear at the same frequency in these measurements. The second singular value seems to show a coherent peak at 0.96 Hz, indicating that two modes are present at this peak. Each of these modes are expected to appear at modulations of this frequency: 0.96 + $n$0.201Hz as well. Any modulations below 0.96 Hz would be obscured by the harmonics of the rotor frequency, but two harmonics are visible at 1.16 and 1.36 Hz. However, only one singular vector is visible at each of those peaks, suggesting that one of the two modes is obscured by noise at those frequencies due to the non-ideal nature of the input spectrum.

In order to quantify these modes, the OMA-EMIF algorithm was applied to the peaks at 0.96 Hz and 1.36 Hz. Two modes were identified at the former frequency and one at the latter with natural frequencies 0.9623, 0.9636, and 1.366 Hz. The corresponding mode vectors are shown in Table 6. The magnitude and phase (in degrees) of each Fourier coefficient is shown. The first mode (0.9323 Hz) shows significant harmonics at $n$=0 and $n$=2, the latter being about 6-7% of the former in magnitude. The other harmonics seem to be caused by noise in the measurements. In contrast, the second mode (0.9636 Hz) only has significant Fourier coefficients for $n$=0; all of its other Fourier coefficients seem to be at the level of the noise. The coefficients identified at 1.366 Hz are due to a modulation of one or both of the first two modes by twice the rotational frequency. Their Fourier coefficients have been shifted (e.g. to account for $l$ in eq. (10)) so that they can be compared with the other two modes. The resulting harmonics agree very well with those for the first mode in both magnitude and phase. This suggests that the mode identified at 1.366 Hz is merely a replicate of the 0.9323 Hz mode due to the modulation in eq. (7).

These results agree very well with what would be expected for a turbine such as this. The phases of the $n$=0 harmonics of the first mode decrease from blade 1 to 2 to 3, revealing that this is a forward whirling mode. Its $n$=2 harmonics show phase angles that increase from blade 1 to 2 to 3, indicating that the $n$=2 harmonics are a backward whirling component of this forward whirling mode. This same behaviour was observed for a simulated turbine in [2] and arises due to the anisotropy of the tower. The phases of the $n$=0 harmonic of the second mode reveal that this mode is a backward whirling mode. None of the other harmonics for that mode show the expected phase relationship, so they are all most likely due to noise.

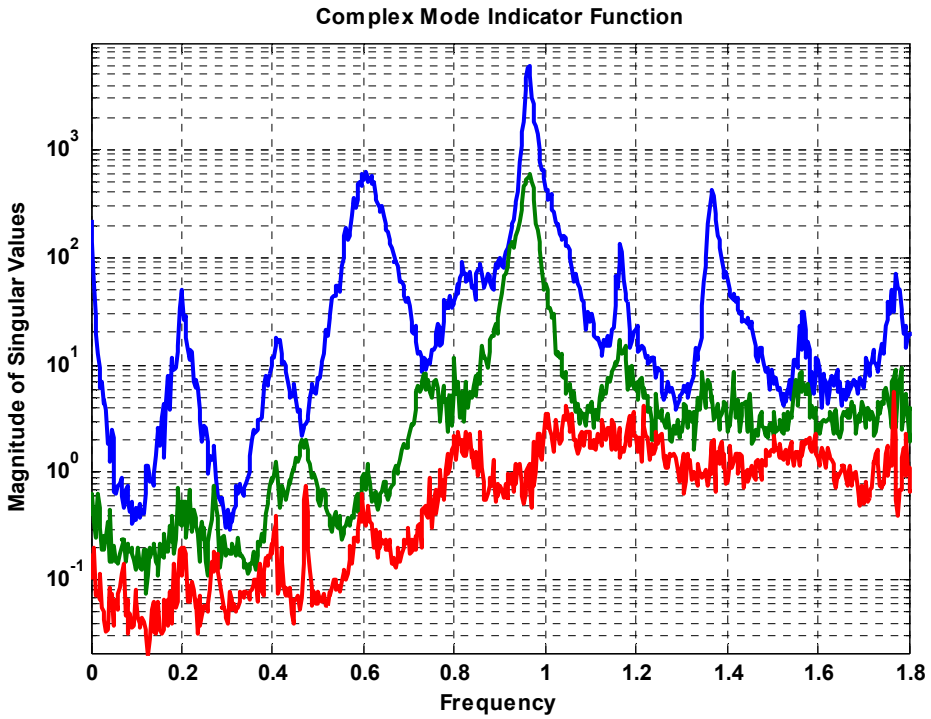


*Figure 5: CMIF of the HPSD for edgewise motion of the three blades of the wind turbine.*

| | | 0.9623 Hz, M1 | | 0.9636 Hz, M2 | | 1.366 Hz | |
|---|---|---|---|---|---|---|---|
| **n** | **Blade** | Mag | Phs (°) | Mag | Phs (°) | Mag | Phs (°) |
| **-2** | **B1** | 0.023 | -174 | 0.123 | -158 | - | - |
| **-2** | **B2** | 0.024 | -179 | 0.142 | -165 | - | - |
| **-2** | **B3** | 0.024 | -175 | 0.116 | -171 | - | - |
| **-1** | **B1** | 0.017 | -4 | 0.040 | 19 | - | - |
| **-1** | **B2** | 0.006 | 139 | 0.036 | 110 | - | - |
| **-1** | **B3** | 0.018 | -78 | 0.028 | -88 | - | - |
| **0** | **B1** | 1 | 0 | 1 | 0 | 1 | 0 |
| **0** | **B2** | 0.957 | -121 | 1.039 | 119 | 0.948 | -122 |
| **0** | **B3** | 0.964 | 122 | 1.045 | -117 | 0.946 | 122 |
| **1** | **B1** | 0.025 | -117 | 0.015 | -123 | 0.022 | -117 |
| **1** | **B2** | 0.022 | -114 | 0.032 | 54 | 0.020 | -108 |
| **1** | **B3** | 0.015 | -135 | 0.036 | -29 | 0.016 | -126 |
| **2** | **B1** | 0.068 | -102 | 0.006 | 50 | 0.072 | -102 |
| **2** | **B2** | 0.070 | 21 | 0.011 | 0 | 0.072 | 21 |
| **2** | **B3** | 0.067 | 138 | 0.009 | 15 | 0.069 | 138 |
| **3** | **B1** | - | - | - | - | 0.002 | -73 |
| **3** | **B2** | - | - | - | - | 0.003 | 125 |
| **3** | **B3** | - | - | - | - | 0.008 | 64 |

*Table 6: Fourier coefficients identified from the HPSD using the OMA-EMIF method.*

## 4. CONCLUSIONS

This paper has extended several advanced methods for operational modal analysis to linear time periodic systems. Curve fitting methods were demonstrated both on the harmonic autospectrum and the positive harmonic autospectrum. The latter were found to be simpler to curve fit and to produce good agreement between the reconstructed and measured positive autospectra. Even then, both methods were found to identify natural frequencies, damping ratios

and mode shapes of similar quality. On the other hand, when the curve fitting methods were applied to very weak peaks in the harmonic autospectra, both methods gave overly large estimates for the Fourier coefficients that were buried in the noise. In this respect, the peak picking method was preferred for these very weak peaks. In any event, it seems advisable to question the accuracy of any Fourier coefficient that is not well represented in the spectrum.

The methods were also applied to simulated measurements from a 5MW wind turbine which was rotating at constant speed. Complex Mode Indicator Functions were formed from the measurements and shown to reveal many of the modes of the turbine, including the first edgewise modes of the turbine, which are of special interest since they tend to be lightly damped and hence can limit the life of the turbine. The OMA-EMIF method was also applied to the measurements and was successful in extracting the forward and backward whirling modes, both of which appeared at the same frequency in the blade measurements. This method proved to a significant aide; in the authors previous work [5, 6] the shapes identified by peak picking were shown and with that method it was very difficult to separate those two modes.

## 5. ACKNOWLEDGEMENT

The first author was supported by the National Science Foundation under Grant CMMI-0969224 while completing this work.

## 6. REFERENCES

[1] K. Stol, M. Balas, and G. Bir, "Floquet modal analysis of a teetered-rotor wind turbine," *Journal of Solar Energy Engineering-Transactions of the ASME,* vol. 124, pp. 364-371, Nov 2002.

[2] P. F. Skjoldan and M. H. Hansen, "On the similarity of the Coleman and Lyapunov-Floquet transformations for modal analysis of bladed rotor structures," *Journal of Sound and Vibration,* vol. 327, pp. 424-439, 2009.

[3] I. Bucher and O. Shomer, "Detecting asymmetry in rotating structures a combined acutation and signal processing approach," in *23rd International Modal Analysis Conference (IMAC XXIII)* Orlando, Florida, 2005.

[4] M. S. Allen and M. W. Sracic, "A New Method for Processing Impact Excited Continuous-Scan Laser Doppler Vibrometer Measurements," *Mechanical Systems and Signal Processing,* vol. 24, pp. 721–735, 2010.

[5] M. S. Allen, M. W. Sracic, S. Chauhan, and M. H. Hansen, "Output-Only Modal Analysis of Linear Time Periodic Systems with Application to Wind Turbine Simulation Data," in *28th International Modal Analysis Conference (IMAC XXVIII)* Jacksonville, Florida, 2010.

[6] M. S. Allen, M. W. Sracic, S. Chauhan, and M. H. Hansen, "Output-Only Modal Analysis of Linear Time Periodic Systems with Application to Wind Turbine Simulation Data," *Mechanical Systems and Signal Processing,* vol. submitted Oct. 2010, 2010.

[7] M. O. L. Hansen, J. N. Sørensen, S. Voutsinas, N. Sørensen, and H. A. Madsen, "State of the art in wind turbine aerodynamics and aeroelasticity," *Progress in Aerospace Sciences,* vol. 42, pp. 285-330, 2006.

[8] S. Yang and M. S. Allen, "Output-Only Modal Analysis Using Continuous-Scan Laser Doppler Vibrometry and Application to a 20kW Wind Turbine," in *29th International Modal Analysis Conference (IMAC XXIX)* Jacksonville, Florida, 2011.

[9] S. Chauhan, R. Martell, D. L. Brown, and R. J. Allemang, "Considerations in the Application of Spatial Domain Algorithms to Operational Modal Analysis," in *International Seminar on Modal Analysis* Leuven, Belgium, 2006.

[10] J. S. Bay, *Fundamentals of Linear State Space Systems*. Boston: McGraw-Hill, 1999.

[11] M. S. Allen, "Frequency-Domain Identification of Linear Time-Periodic Systems using LTI Techniques," *Journal of Computational and Nonlinear Dynamics* vol. 4, 24 Aug. 2009.
[12] M. Allen and J. H. Ginsberg, "Floquet Modal Analysis to Detect Cracks in a Rotating Shaft on Anisotropic Supports," in *24th International Modal Analysis Conference (IMAC XXIV)* St. Louis, MO, 2006.
[13] M. S. Allen and J. H. Ginsberg, "A Global, Single-Input-Multi-Output (SIMO) Implementation of The Algorithm of Mode Isolation and Applications to Analytical and Experimental Data," *Mechanical Systems and Signal Processing,* vol. 20, pp. 1090–1111, 2006.
[14] M. S. Allen and J. H. Ginsberg, "Global, Hybrid, MIMO Implementation of the Algorithm of Mode Isolation," in *23rd International Modal Analysis Conference (IMAC XXIII)* Orlando, Florida, 2005.
[15] R. J. Allemang and D. L. Brown, "A Unified Matrix Polynomial Approach to Modal Identification," *Journal of Sound and Vibration,* vol. 211, pp. 301-322, 1998.
[16] D. Tcherniak, S. Chauhan, and M. H. Hansen, "Applicability limits of Operational Modal Analysis to Operational wind turbines," in *28th International Modal Analysis Conference (IMAC XXVIII)* Jacksonville, Florida, 2010.